Features of hadronic and deconfined matter in a range of collision energies spanning from the BNL Alternating Gradient Synchrotron to the CERN Large Hadron Collider

M. Petrovici* and A. Pop

National Institute for Physics and Nuclear Engineering (IFIN-HH), P.O. Box MG-6, Hadron Physics Department, Măgurele, Romania

(Received 21 September 2022; accepted 3 February 2023; published 17 March 2023)

Previous extensive studies on the dependence of the average transverse momentum, its slope as a function of the hadron mass, and the average transverse expansion on the particle multiplicity per unit rapidity and unit transverse overlap area of the colliding partners are extended to the ratio of the energy density to the entropy density. The behavior of the ratio between the average transverse momentum and the square root of the particle multiplicity per unit rapidity and unit transverse overlap area $\langle p_T\rangle/\sqrt{\langle dN/dy\rangle/S_\perp}$ as a function of collision energy for a given centrality or as a function of centrality for a given collision energy supports the predictions of color glass condensate and percolation based approaches. The dependence of the ratio of the energy density $\langle dE_T/dy\rangle/S_\perp$ to the entropy density $\langle dN/dy\rangle/S_\perp$ at different collision centralities for *A*-*A* collisions from the Alternating Gradient Synchrotron, the Super Proton Synchrotron, the BNL Relativistic Heavy Ion Collider, and the CERN Large Hadron Collider energies is presented. The trend of this ratio towards a plateau at the highest RHIC energies followed by a steep rise at LHC energies is in agreement with theoretical predictions made 40 years ago that indicate this behavior as a signature of a phase transition. This pattern strongly depends on the collision geometry, converging towards the dependence that characterizes the *pp* minimum bias collisions for the most peripheral *A*-*A* collisions. Expected similarities between *pp* and Pb-Pb collisions at LHC energies are confirmed.

DOI: 10.1103/PhysRevC.107.034913

I. INTRODUCTION

The unprecedented amount of experimental information obtained at the energies available at the Alternating Gradient Sychrotron (AGS), the Super Proton Synchrotron (SPS), and the BNL Relativistic Heavy Ion Collider (RHIC) up to the highest energies available at the CERN Large Hadron Collider (LHC) supports the theoretical predictions made about 50 years ago on the possibility to produce very hot and dense matter in heavy-ion collisions [1]. Using Quantum Chromo-Dynamics (QCD) asymptotic freedom properties, a transition from the hadronic phase to a high-density "quark soup" [2,3] or "quark-gluon plasma" [4] following the "quark liberation" idea [3] is expected. The first estimates of the transition from a gas of free nucleons to hadronic matter and subsequently to deconfined matter as a function of density were done within the percolation approach [5,6]. Studying the production mechanism and properties of tiny pieces of deconfined matter as a function of temperature and density is a difficult task to the extent that the highly inhomogeneous initial state, finite-size effects, and violent dynamical evolution must be taken into account to obtain a unique explanation of the experimental observations. That is why a clean and unambiguous experimental signature of deconfinement using collisions with heavy ions is rather difficult to establish. Theoretical approaches, which combine sound hypotheses for different snapshots of the formation and evolution of the system produced in heavy-ion collisions starting with the initial phase described in the color glass condensate (CGC) approach [7–10], followed by the process of equilibration described on the basis of the QCD kinetic theory method and the hydrodynamic expansion, were recently developed [11]. The correlation between the multiplicity of particles and the average transverse momentum ($\langle p_T\rangle$) has been proposed as a signature of the transition from hadronic to deconfined matter [12]. Such phenomenological models predict an increase followed by a plateau of the $\langle p_T\rangle$ as a function of entropy density, caused by the mixed phase corresponding to the transition from pure hadronic matter to deconfined matter. At even larger entropy density, the $\langle p_T\rangle$ starts to increase again. Following this idea and existing information on the average transverse mass ($\langle m_T\rangle$) of charged hadrons identified in *A*-*A* collisions at AGS, SPS, and RHIC, a saturation of the $\langle m_T\rangle$ as a function of the charged-particle multiplicity per unit rapidity for the most-central collisions was evidenced [13]. In this study the $\langle m_T\rangle$ was estimated using an exponential parametrization of the experimental p_T spectra. Recently, including more information obtained at RHIC in the Beam Energy Scan (BES) program for Au-Au collisions and LHC data for the Pb-Pb collision at $\sqrt{s_{NN}} =$

*mpetro@nipne.ro

2.76 TeV [14] the correlation $(\langle m_T\rangle - m_0)$-$\ln(\sqrt{s_{NN}})$ for the most-central collisions was studied for identified hadrons under the hypothesis that $(\langle m_T\rangle - m_0)$ can be an approximation of the system temperature, while $\ln(\sqrt{s_{NN}}) \sim \langle dN/dy\rangle$ can be an approximation of its entropy. m_0 is the rest mass of the particle. A dependence on mass was clearly observed. The saturation range in $\ln(\sqrt{s_{NN}})$ decreases and $(\langle m_T\rangle - m_0)$ increases again more violently going from pions to protons. It is worth mentioning that collective expansion and suppression phenomena can contribute in such a correlation to the observed trend. A similar prediction was obtained by including the relativistic hydrodynamic evolution of the quark-gluon plasma [15,16]. In these works it was suggested that the correlation between the ratio of the energy density to entropy density is also sensitive to the transition from hadronic to deconfined matter. The energy density per unit transverse overlap area can be estimated using the Bjorken invariance, while the entropy density per unit transverse overlap area, assuming an isentropic expansion, is proportional to the particle multiplicity per unit rapidity and unit transverse overlap area. A similar correlation, using the charged-particle multiplicity and the transverse energy per unit pseudorapidity $(\langle dE_T/d\eta\rangle/\langle dN_{ch}/d\eta\rangle)$ for the most-central collisions, with the assumption that $\ln(\sqrt{s_{NN}}) \sim dN_{ch}/d\eta$ and of a rather small dependence of the transverse overlap area $(S_\perp)$ on the collision energy, was plotted using experimental information from SIS18 up to the highest energy from RHIC [17], the results from the LHC for the Pb-Pb collision at $\sqrt{s_{NN}} = 2.76$ TeV being included once the data became available [18]. As predicted by the abovementioned models a plateau at the highest energies at RHIC and a strong increase at the LHC energy were evidenced. The $\langle dE_T/d\eta\rangle/\langle dN_{ch}/d\eta\rangle$-$\sqrt{s_{NN}}$ correlations for the most-central collisions were shown for data measured by the PHENIX Collaboration at RHIC energies [19]. The $\langle dE_T/dy\rangle/\langle dN_{ch}/dy\rangle$-$\sqrt{s_{NN}}$ correlations for different centralities were represented for data measured by the STAR Collaboration at BES energies [20]. Theoretical predictions show that the energy over entropy versus entropy correlation is more sensitive to the equation of state than the average transverse mass versus multiplicity density one [21].

In the present paper, the results for the $\langle dE_T/dy\rangle/\langle dN/dy\rangle$-$\langle dN/dy\rangle/S_\perp$ correlation as a function of centrality in *A*-*A* collisions at different energies and a comparison with *pp* minimum bias and *pp* as a function of $\langle dN/dy\rangle/S_\perp$ at LHC energies are presented. Results based on published data obtained in Au-Au collisions at AGS and RHIC and Pb-Pb collisions at SPS and LHC, in terms of $\langle dE_T/dy\rangle/\langle dN/dy\rangle$-$\langle dN/dy\rangle/S_\perp$ for the most-central collisions, are presented in Sec. II. Section III is dedicated to similar studies as a function of centrality for RHIC and LHC energies. In Sec. IV the core contribution in such correlations is presented. The dependence on $\langle dN/dy\rangle/S_\perp$ of the Bjorken energy density times the interaction time for central collisions and as a function of centrality is presented in Sec. V. The comparison of *A*-*A* with minimum bias (MB) *pp* collisions at the same energies and for different charged-particle multiplicities at LHC energies is discussed in Sec. VI. Conclusions are presented in Sec. VII.

II. $\langle dE_T/dy\rangle/\langle dN/dy\rangle$-$\langle dN/dy\rangle/S_\perp$ CORRELATION FOR CENTRAL *A*-*A* COLLISIONS

In our previous studies [22–24] it was shown that the particle multiplicity per unit rapidity and unit transverse overlap area, a good estimate of the entropy density, turns out to be a scaling observable that governs the behavior of the average transverse expansion for identified charged hadrons and hyperons, independent of the size of the colliding systems and even for *pp* collisions at LHC energies. For collision energies higher than $\sqrt{s_{NN}} = 39$ GeV, the scaling was also evident for the slope of the $\langle p_T\rangle$ as a function of mass. While such scaling also occurs below $\sqrt{s_{NN}} = 39$ GeV up to the mid-central collisions, a slight deviation of ≈10% relative to the higher energies is observed towards central collisions. As far as concerns the $\langle p_T\rangle$, a very good scaling is observed for the identified charged hadrons at the RHIC energies. The linear dependence of the $\langle p_T\rangle$ on $\sqrt{\langle dN/dy\rangle/S_\perp^{\rm geom}}$ holds also for LHC energies, with a slightly different offset relative to the RHIC energies and a tendency towards saturation at the most-central collisions. The geometrical transverse overlap area $(S_\perp^{\rm geom})$ of the two colliding nuclei for a given incident energy and centrality was estimated on the basis of a Glauber Monte-Carlo (MC) approach [25–28] as explained in Ref. [22] where its values were compiled. They are used in the estimates made in the present paper. Using also the experimental $\langle p_T\rangle$ values for positive pions, kaons, and protons and the $\langle dN/dy\rangle$ values compiled in Ref. [22], in Fig. 1(a) is represented the ratio $\langle p_T\rangle/\sqrt{\langle dN/dy\rangle/S_\perp^{\rm geom}}$ as a function of collision energy for different centralities, while in Fig. 1(b) the ratio is presented as a function of centrality $(\langle N_{\rm part}\rangle)$ for different collision energies. As can be seen in Fig. 1, the ratio between the average transverse momentum and the square root of the hadron multiplicity per unit rapidity and unit transverse overlap area of the colliding nuclei decreases towards central collisions and higher energies, thus supporting the predictions based on color field description of the small x degrees of freedom [7,10,29,30], the local parton-hadron duality picture [31], and the dimensionality argument [32,33].

A similar behavior is predicted by the string percolation scenario, inspired by the CGC approach [34,35]. In a string percolation approach [35],

$$\frac{dN}{dy} = F(\eta)\bar{N}^s\mu_0, \tag{1}$$

$$\langle p_T^2\rangle = \langle p_T^2\rangle_1/F(\eta). \tag{2}$$

The color reduction factor

$$F(\eta) \equiv \sqrt{\frac{1-e^{-\eta}}{\eta}}, \tag{3}$$

where η, the two-dimensional transverse density of strings, is given by $\eta \equiv (r_0/R)^2\bar{N}^s$, r_0 being the string radius and R the radius of the transverse overlap region. $\bar{N}^s$ is the average number of strings, μ_0 and $\langle p_T^2\rangle_1$ are respectively the average particle density and the average transverse momentum squared of a single string. Therefore, $\sqrt{\langle p_T^2\rangle}/\sqrt{\langle dN/dy\rangle/S_\perp} \approx 1/\sqrt{(1-e^{-\eta})}$ is decreasing with

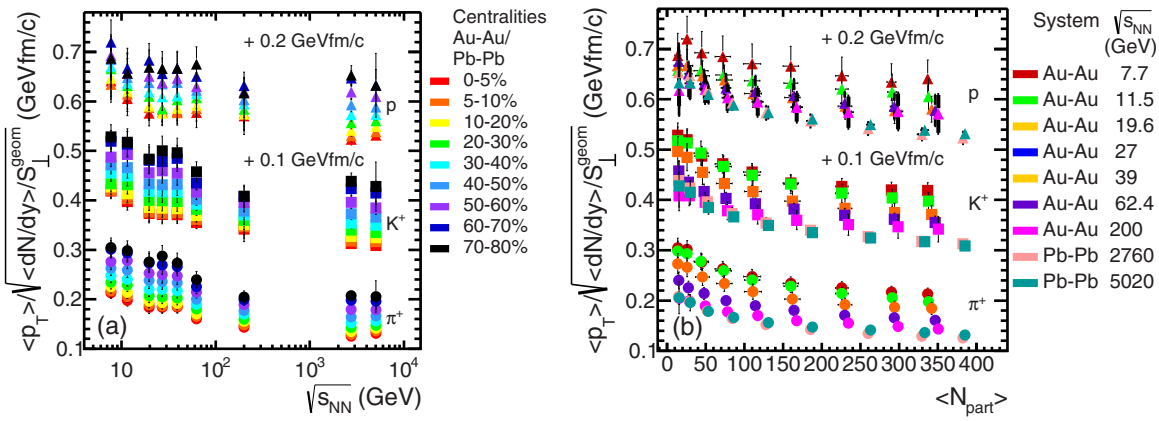

FIG. 1. $\langle p_T\rangle/\sqrt{\langle dN/dy\rangle/S_\perp^{\rm geom}}$ dependence on (a) collision energy for different centralities and (b) $\langle N_{\rm part}\rangle$ for different collision energies.

centrality for a given collision energy and with the collision energy for a given centrality. The effects of the strong longitudinal color fields on the identified charged hadrons and hyperons p_T distributions in pp collisions at $\sqrt{s} = 7$ TeV have also been investigated within the framework of the HIJING/B$\bar{B}$ v2.0 model [36]. The experimental ratios of the p_T distributions at different charged-particle multiplicities to the one corresponding to the MB pp collision, each of them normalized to the corresponding charged-particle density, were well reproduced using an increased strength of the color field, characterized by the effective values of the string tension, from low to high charged-particle multiplicity. These results point out the necessity of introducing a multiplicity (or energy density) dependence for the effective value of the string tension. They also show that at the LHC energies the global features of the interactions are mainly determined by the properties of the initial chromoelectric flux tubes, the system size playing a minor role. A rough estimate of the gluon number density and the occupation number in the early stage of relativistic heavy-ion collisions, following Ref. [37], gives values of 2.3 (2.9) higher at $\sqrt{s_{NN}} = 2.76$ TeV (5.02 TeV) Pb-Pb central collisions relative to Au-Au central collisions at $\sqrt{s_{NN}} = 200$ GeV. For the largest charged-particle multiplicity in pp collisions at $\sqrt{s} = 7$ TeV, the values are a bit larger than those corresponding to Pb-Pb central collisions at $\sqrt{s_{NN}} = 5.02$ TeV. The parton density evolution as a function of x and Q^2, addressed more than 35 years ago [38], was experimentally confirmed at HERA [39]. The rise of the structure function at low x is still visible at small values of Q^2 [40,41] where the perturbative QCD does not work anymore. Therefore, rich and short-lived partonic cascades become visible as the collision energy increases, with the string density and the percolation probability increasing too. The approaches mentioned above predict an increase of the average transverse momentum at the same particle multiplicity per unit rapidity and unit transverse overlap area with collision energy and system size independence of the global features evidenced at LHC energies, the properties of the initial color electromagnetic flux tubes playing the main role.

The $\langle dE_T/dy\rangle/\langle dN/dy\rangle$-$\langle dN/dy\rangle/S_\perp$ correlation for the most-central A-A collisions using the experimental information collected over the years starting from AGS up to the LHC energies is presented in Fig. 2. In the case of RHIC and LHC, experimental data from the STAR and ALICE Collaborations were used mainly due to the availability in terms of measured spectra for light-flavor hadrons. The transverse energy per unit rapidity was considered in two ways. In case I [Fig. 2(a)] published measured values were used when they were available, while in case II [Fig. 2(b)] an approximation similar to that from Ref. [42] was applied for the $\langle dE_T/dy\rangle$ calculation. For the AGS and SPS energies, the $\langle dE_T/d\eta\rangle$ values and the scaling factor for the η to y transition at midrapidity were taken from Ref. [17] for all cases. For the BES energies, the STAR data from Ref. [20] were used in case I. It should be noted that these were obtained from the transverse momentum spectra measured up to Λ particles. For higher energies, STAR data regarding $\langle dE_T/dy\rangle$ reported for Au-Au at $\sqrt{s_{NN}} = 62.4$ GeV in Refs. [43,44] and at $\sqrt{s_{NN}} = 200$ GeV in Ref. [45], as well as the results of the transverse energy measurement for Pb-Pb at $\sqrt{s_{NN}} = 2.76$ TeV from Ref. [18], were considered. In case II, the full formula used to approximate dE_T/dy was

$$\frac{dE_T}{dy} \simeq \frac{3}{2}\left(\langle m_T\rangle\frac{dN}{dy}\right)^{(\pi^+ + \pi^-)} + 2\left(\langle m_T\rangle\frac{dN}{dy}\right)^{(p+\bar{p},\,\Xi^- + \bar{\Xi}^+)} + \left(\langle m_T\rangle\frac{dN}{dy}\right)^{(K^+ + K^-,\,\Lambda+\bar{\Lambda},\,\Omega^- + \bar{\Omega}^+)} + 2\left(\langle m_T\rangle\frac{dN}{dy}\right)^{K_S^0} + 2\left(\langle m_T\rangle\frac{dN}{dy}\right)^{(\Sigma^+ + \Sigma^-)}. \quad (4)$$

When the particle spectra were available, the average transverse mass was calculated. For Pb-Pb at $\sqrt{s_{NN}} = 5.02$ TeV in the case of strange and multistrange particles for which the transverse momentum distributions have not yet been published, the approximation $\langle m_T\rangle = \sqrt{\langle p_T^2\rangle + m_0^2}$ was used. In accordance with the convention made in calorimetric measurements, $\langle m_T\rangle$ was replaced by $\langle m_T\rangle - m_0$ for baryons and by $\langle m_T\rangle + m_0$ for antibaryons. In both cases the particle multiplicity per unit rapidity, dN/dy was estimated

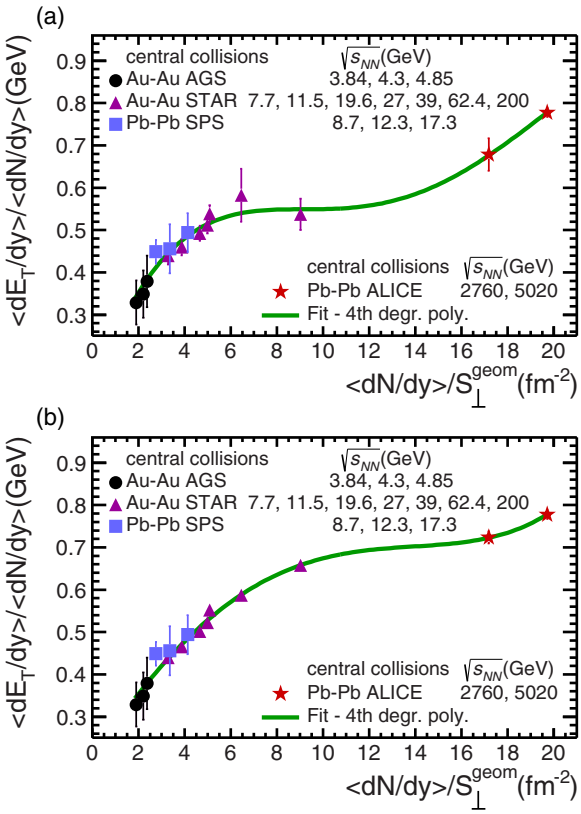

FIG. 2. The $\langle dE_T/dy\rangle/\langle dN/dy\rangle$)-$\langle dN/dy\rangle/S_\perp$ correlation for the most-central A-A collisions for (a) case I and (b) case II. The two representations are quite different at the highest energies from RHIC. This is mainly due to the difference at $\sqrt{s_{NN}} = 200$ GeV between the transverse energy measured in Ref. [45] (case I) and the one estimated in this paper from the existing particle spectra (case II). The difference is about 20%, the largest compared to the other energies, while the $\langle dN/dy\rangle$ value is the same. For the AGS and SPS energies, since only one set of data is available, taken from Ref. [17], the two cases coincide. The continuous lines, used to guide the eye, represent the results of fourth-degree polynomial fits of the experimental points.

according to

$$\frac{dN}{dy} \simeq \frac{3}{2}\frac{dN}{dy}^{(\pi^+ + \pi^-)} + 2\frac{dN}{dy}^{(p+\bar{p},\Xi^- + \bar{\Xi}^+)} + \frac{dN}{dy}^{(K^+ + K^-,\Lambda+\bar{\Lambda},\Omega^- + \bar{\Omega}^+)} + 2\frac{dN}{dy}^{K_S^0} + 2\frac{dN}{dy}^{(\Sigma^+ + \Sigma^-)} \quad (5)$$

The experimental data in terms of transverse momentum spectra, yields, and average transverse momenta were taken from Ref. [46] (AGS and SPS), Refs. [14,47] (Au-Au, BES), Refs. [42,48] (Au-Au at $\sqrt{s_{NN}} = 62.4$ GeV), Refs. [42,49,50] (Au-Au at $\sqrt{s_{NN}} = 200$ GeV), Refs. [51–53] (Pb-Pb at $\sqrt{s_{NN}} = 2.76$ TeV), and Refs. [54–57] (Pb-Pb at $\sqrt{s_{NN}} = 5.02$ TeV). Equations (4) and (5) were applied so that the same particles and antiparticles were taken into consideration in both formulas depending, from system to system and case to case, on the most complete published experimental information. With the increase of the collision energy, the contribution

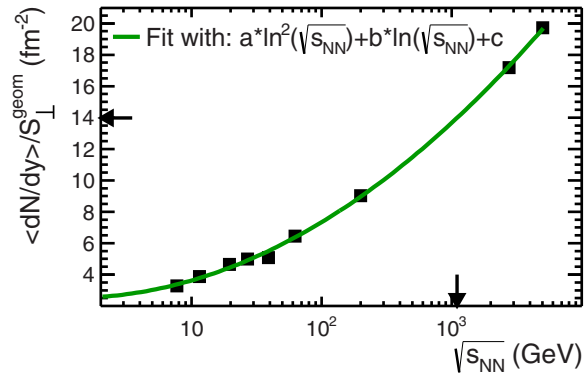

FIG. 3. $\langle dN/dy\rangle/S_\perp^{\rm geom}$ as a function of collision energy. The collision energy values correspond to the $\langle dN/dy\rangle/S_\perp^{\rm geom}$ values from Fig. 2. The line is the result of the fit with a second-order polynomial in $\ln(\sqrt{s_{NN}})$. The two arrows that point to the x and y axes indicate the approximate value of the collision energy and $\langle dN/dy\rangle/S_\perp^{\rm geom}$, respectively, at the inflection point in case II.

of strange and multistrange particles in the formulas becomes more and more important. Thus, for Au-Au at $\sqrt{s_{NN}} = 62.4$ and $\sqrt{s_{NN}} = 200$ GeV and Pb-Pb at both LHC energies, the contribution of Σ particles was also considered as explained in Refs. [18,58]. In Fig. 2, $\langle dE_T/dy\rangle/\langle dN/dy\rangle$ as a function of $\langle dN/dy\rangle/S_\perp$ for the most-central collisions is shown. The continuous lines in the figures, used to guide the eye, are the results of the fits of experimental points using a fourth-degree polynomial. $\langle dE_T/dy\rangle/\langle dN/dy\rangle$ increases with $\langle dN/dy\rangle/S_\perp$ from AGS to SPS and RHIC energies, up to $\sqrt{s_{NN}} = 39$ GeV. Above $\sqrt{s_{NN}} = 39$ GeV, the slope changes and a tendency towards saturation is evident. Even if the gap in the collision energy between $\sqrt{s_{NN}} = 200$ GeV, the highest one at RHIC, and the LHC energies is rather large, it is obvious that the result of the extrapolation of the trend of experimental data from low energies is below the values of the experimental data corresponding to $\sqrt{s_{NN}} = 2.76$ TeV and 5.02 TeV LHC energies. The second rise taken at the inflection point in case II [Fig. 2(b)] corresponds approximately to the rise point, at the end of the plateau, in case I [Fig. 2(a)], being around $\sqrt{s_{NN}} = 1100$ GeV, as deduced from the representation of $\langle dN/dy\rangle/S_\perp^{\rm geom} = f(\sqrt{s_{NN}})$ in Fig. 3. As can be seen in Sec. V, this value agrees with the one corresponding to similar trends evidenced in the behavior of the slope of the dependence of the Bjorken energy density times the interaction time on the entropy density, as a function of the collision energy. Experimental measurements between $\sqrt{s_{NN}} = 200$ GeV and 2760 GeV, missing for the moment, would be of real interest in this context. Less influenced by processes such as collective expansion, suppression or kinematic cuts, the behavior of such a representation supports the theoretical predictions that identify it as a signature of the phase transition [15,16]. The obvious rise at LHC energies could be the result of the combined contributions of a higher temperature of the deconfined medium and a higher percolation probability in the regions of high-density color electromagnetic fields.

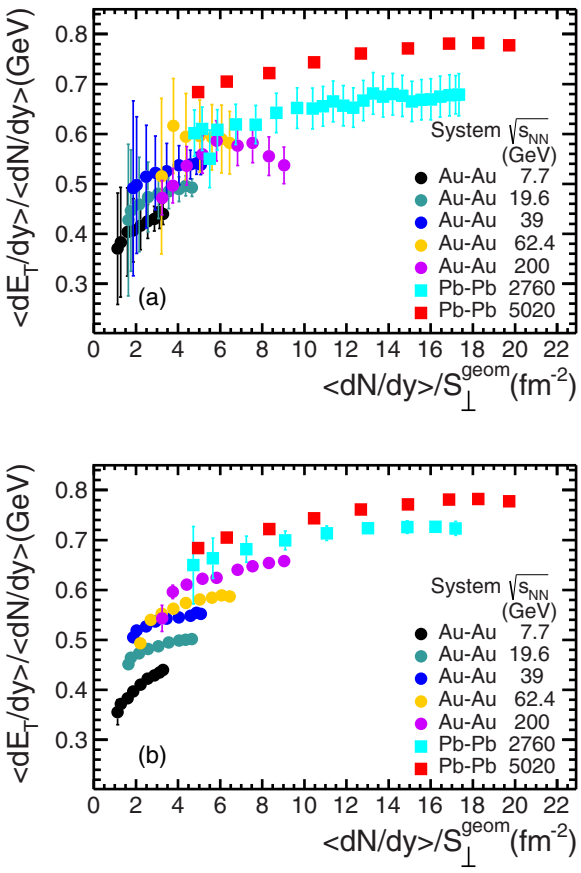

FIG. 4. The $\langle dE_T/dy\rangle/\langle dN/dy\rangle$-$\langle dN/dy\rangle/S_\perp$ correlation for different collision energies and different centralities for (a) case I and (b) case II.

III. $\langle dE_T/dy\rangle/\langle dN/dy\rangle$-$\langle dN/dy\rangle/S_\perp$ CORRELATION FOR DIFFERENT CENTRALITIES AT RHIC AND LHC ENERGIES

The $\langle dE_T/dy\rangle/\langle dN/dy\rangle$-$\langle dN/dy\rangle/S_\perp$ correlation depending on the centrality for several collision energies is shown in Fig. 4 where the difference between panels (a) and (b) is the same as that in Fig. 2, as explained in the previous section. A close to linear dependence of $\langle dE_T/dy\rangle/\langle dN/dy\rangle$ as a function of $\langle dN/dy\rangle/S_\perp$ can be seen. The offsets are different, increasing with the collision energy. The $\langle dE_T/dy\rangle/\langle dN/dy\rangle$-$\langle dN/dy\rangle/S_\perp$ correlations for Au-Au at $\sqrt{s_{NN}} = 62.4$ GeV [43,44] and 200 GeV [45] based on calorimetry measurements (case I) do not follow the general trend, what is not observed in case II [Fig. 4(b)]. In Fig. 5 are shown the $\langle dE_T/dy\rangle/\langle dN/dy\rangle$-$\langle dN/dy\rangle/S_\perp$ correlations for the overlap transverse areas $S_\perp \approx 24$, 64, 108, and 149 fm^2. The lines represent the result of fitting the corresponding points with a fourth-degree polynomial. A clear dependence on the size of the transverse overlap area is observed. The rise in $\langle dE_T/dy\rangle/\langle dN/dy\rangle$ at RHIC energies becomes steeper and the range in $\langle dN/dy\rangle/S_\perp$, corresponding to a close to a plateau trend, decreases from central to peripheral collisions [22] and is expected to converge towards the values corresponding to minimum bias pp collisions in the same energy range, once

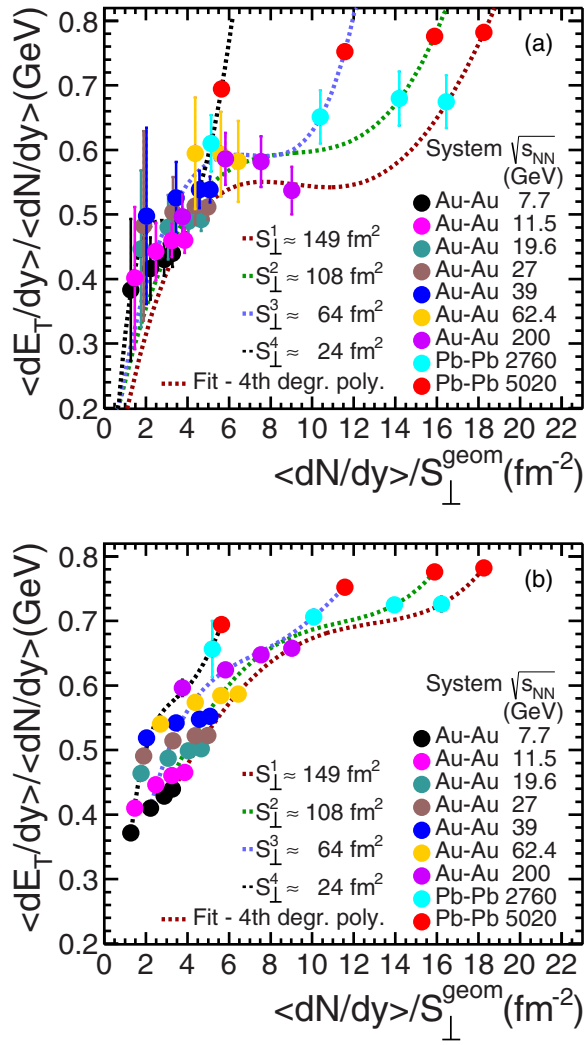

FIG. 5. The $\langle dE_T/dy\rangle/\langle dN/dy\rangle$-$\langle dN/dy\rangle/S_\perp$ correlation for four values of $S_\perp^{\rm geom}$ and different collision energies for (a) case I and (b) case II. The lines represent the results of fourth-degree polynomial fits of the experimental points.

the contribution from nucleons suffering single collisions becomes predominant. At each inflection point of the fit lines, the corresponding $\langle dE_T/dy\rangle/\langle dN/dy\rangle$ value, related to the temperature of the mixed phase up to the pressure contribution, was estimated. The representation of these values as a function of $S_\perp$ shows a decrease from the central collisions to the peripheral ones, as can be seen in Fig. 6. Such a volume dependence was predicted for the chiral phase transition, the critical temperature decreasing towards smaller volume [59,60]. It is worth mentioning that a volume dependence has also been observed in the magnetic phase transition [61]. The pressure term in the equation of state could also contribute to the observed trend. Therefore, theoretical models taking into account all possible contributions needed to reproduce the experimental trend are required.

IV. $(\langle dE_T/dy\rangle/\langle dN/dy\rangle)^{\rm core}$-$(\langle dN/dy\rangle/S_\perp)^{\rm core}$ CORRELATION

In a simple core-corona picture different observables in heavy-ion collisions as a function of centrality and colli-

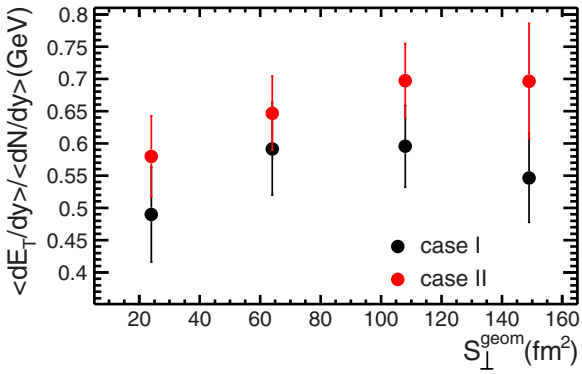

FIG. 6. $\langle dE_T/dy\rangle/\langle dN/dy\rangle$ calculated at the inflection point in the $\langle dE_T/dy\rangle/\langle dN/dy\rangle$-$\langle dN/dy\rangle/S_\perp$ correlation for four values of $S_\perp^{\rm geom}$ and different collision energies. Black symbols correspond to Fig. 5(a) and the red symbols correspond to Fig. 5(b).

sion energy can be seen as the result of the combination between the contribution coming from the interactions of nucleons undergoing only single collisions (corona) and that coming from the multiple interactions of the rest of the nucleons (core). The dependence on the collision energy and the centrality of the core-corona relative weight and its influence on different observables has been studied based on different approaches [62–69]. The transverse overlap areas corresponding to interacting nucleons suffering more than a single collision $[(S_\perp^{\rm geom})^{\rm core}]$ were estimated within the Glauber Monte-Carlo approach and compiled in Ref. [22]. Their $\langle N_{\rm part}\rangle$ dependence is presented in Fig. 7. Because the p_T spectra are not yet published for all hadrons measured in MB pp collisions, the studies whose results are presented in this section were done by using yields and average transverse mass values only for $\pi^\pm$, $K^\pm$, p and $\bar{p}$, and the corresponding neutral hadrons in Eqs. (4) and (5) for both cases, i.e., total and core. The core corresponding yield and

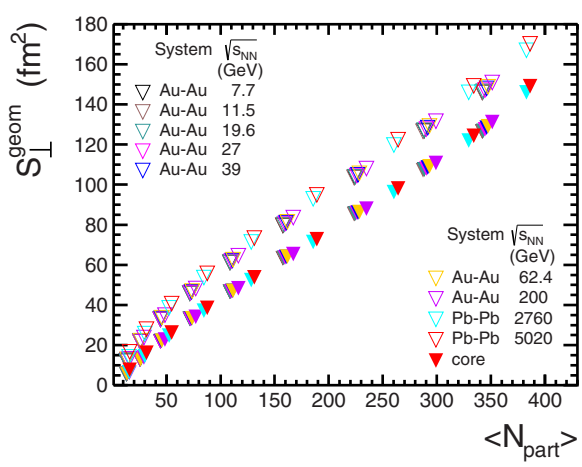

FIG. 7. The transverse overlap area of the colliding nuclei at different energies estimated with the Glauber MC approach corresponding to all nucleons ($S_\perp^{\rm geom}$), open symbols, and to nucleons suffering more than a single collision $[(S_\perp^{\rm geom})^{\rm core}]$, solid symbols, as a function of the number of participants $\langle N_{\rm part}\rangle$.

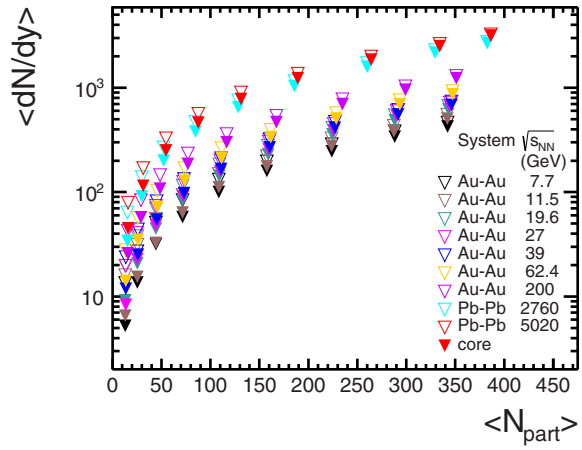

FIG. 8. $\langle dN/dy\rangle$ estimated by considering only $\pi^\pm$, $K^\pm$, p, and $\bar{p}$ and the corresponding neutral hadrons for all A-A collisions at all measured energies; open symbols represent the total contribution, and solid symbols represent the core contribution.

the $\langle m_T\rangle$ for a given species have been estimated by subtracting from the p_T spectra for A-A at a given centrality the corresponding p_T spectra measured in the MB pp collision at the same energy, weighted with the number of nucleons suffering only single collisions [69]. $\langle dN/dy\rangle$ total values and values corresponding to the core contribution are shown in Fig. 8 as a function of total $\langle N_{\rm part}\rangle$. As expected, the corona contribution decreases from peripheral collisions towards central collisions. The total $\langle dE_T/dy\rangle/\langle dN/dy\rangle$-$\langle dN/dy\rangle/S_\perp$ and core $(\langle dE_T/dy\rangle/\langle dN/dy\rangle)^{\rm core}$-$(\langle dN/dy\rangle/S_\perp)^{\rm core}$ correlations for four corresponding overlap areas are presented in Figs. 9(a) and 9(b), respectively. Although they look similar, the dependence on the fireball transverse area is more clearly observed especially at lower values of the transverse overlap area, the tendency towards saturation being enhanced for the core contribution. The quantitative difference can be followed in Fig. 10 where we present the $\langle dE_T/dy\rangle/\langle dN/dy\rangle$ values corresponding to the inflection points of the fit lines for the four values of $S_\perp$, total and core. The decrease from central to peripheral collisions is similar with the trend presented in the previous section where all hadrons were considered. As expected, the main difference between total and core is at peripheral collisions. Nevertheless, the decrease of $\langle dE_T/dy\rangle/\langle dN/dy\rangle$ values corresponding to the inflection points from central (larger $S_\perp$) to peripheral (lower $S_\perp$) is also present when only the core contribution is considered.

V. BJORKEN ENERGY DENSITY AS A FUNCTION OF $\langle dN/dy\rangle/S_\perp$

The Bjorken energy density times the interaction time ($\epsilon_{Bj}\tau$), i.e., $\langle dE_T/dy\rangle/S_\perp$ [42,70], as a function of $\langle dN/dy\rangle/S_\perp$ for the most-central A-A collisions considered in the previous sections is presented in Fig. 11. Figures 11(a) and 11(b) were obtained for cases I and II as discussed in Secs. II and III.

The $\epsilon_{Bj}\tau$ values from AGS, SPS, and RHIC energies have a linear dependence on the particle multiplicity per unit rapidity

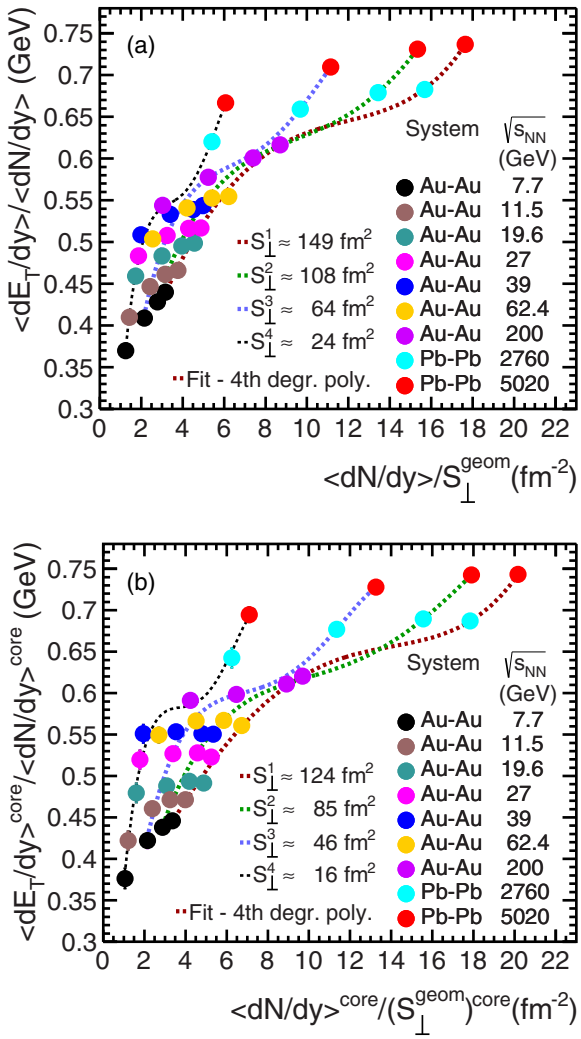

FIG. 9. Total $\langle dE_T/dy\rangle/\langle dN/dy\rangle$-$\langle dN/dy\rangle/S_\perp$ (a) and core $(\langle dE_T/dy\rangle/\langle dN/dy\rangle)^{\text{core}}$-$(\langle dN/dy\rangle/S_\perp)^{\text{core}}$ (b) correlations for four values of the total and core transverse overlap area and different collision energies. The lines are the results of fits with a fourth-order polynomial.

and unit transverse overlap area $\langle dN/dy\rangle/S_\perp$. The extrapolation to the $\langle dN/dy\rangle/S_\perp$ values corresponding to the LHC energies falls below the experimental results. In Fig. 12 are represented the $\epsilon_{Bj}\tau$ values for different centralities and collision energies. Figures 12(a) and 12(b) were obtained for cases I and II as explained in Secs. II and III. For each collision energy, $\epsilon_{Bj}\tau$ shows a linear dependence on $\langle dN/dy\rangle/S_\perp$. The values of the slope of this dependence, related to the temperature of the system, resulting from a linear fit of this correlation for each system and energy, as a function of collision energy are presented in Fig. 13. The slope values increase from AGS energies to the highest RHIC energy. The values for LHC energies are larger and not in-line with what should be expected from a simple extrapolation of the trend observed at lower collision energies, thus suggesting a saturation or an inflection point within the energy gap between RHIC and LHC energies. Following the considerations presented in Sec. II, the physics behind the increasing trend at LHC energies could be related

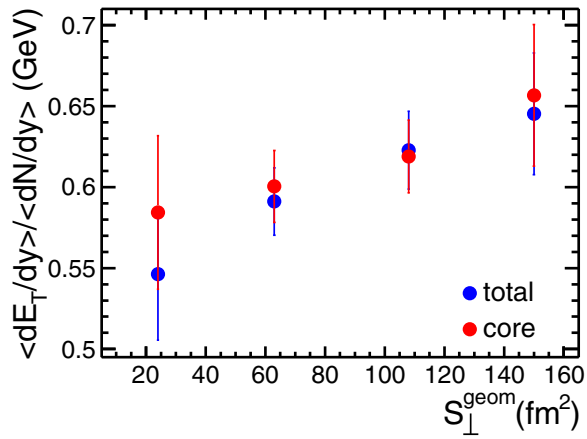

FIG. 10. $\langle dE_T/dy\rangle/\langle dN/dy\rangle$ calculated at the inflection point in the $\langle dE_T/dy\rangle/\langle dN/dy\rangle$-$\langle dN/dy\rangle/S_\perp$ total and core correlations (total correlations are represented by blue symbols; core correlations are represented by red symbols) for four values of the transverse overlap area and different collision energies, as a function of the total transverse overlap area.

to the large increase of the gluon density, therefore increasing the percolation probability, the ropes decay being at the origin of increased average transverse momentum.

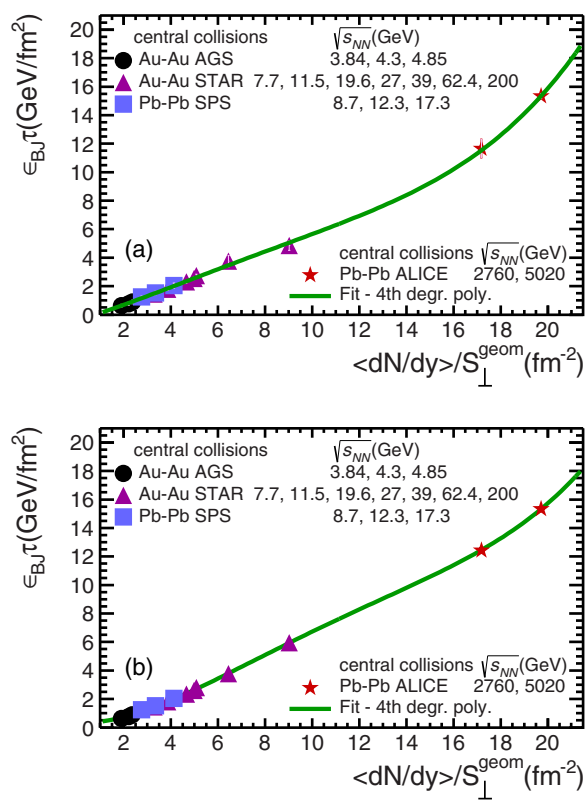

FIG. 11. The Bjorken energy density times the interaction time as a function of $\langle dN/dy\rangle/S_\perp$ for the most-central A-A collisions for (a) case I and (b) case II. The green line is the result of a fit with a fourth-order polynomial, used to guide the eye.

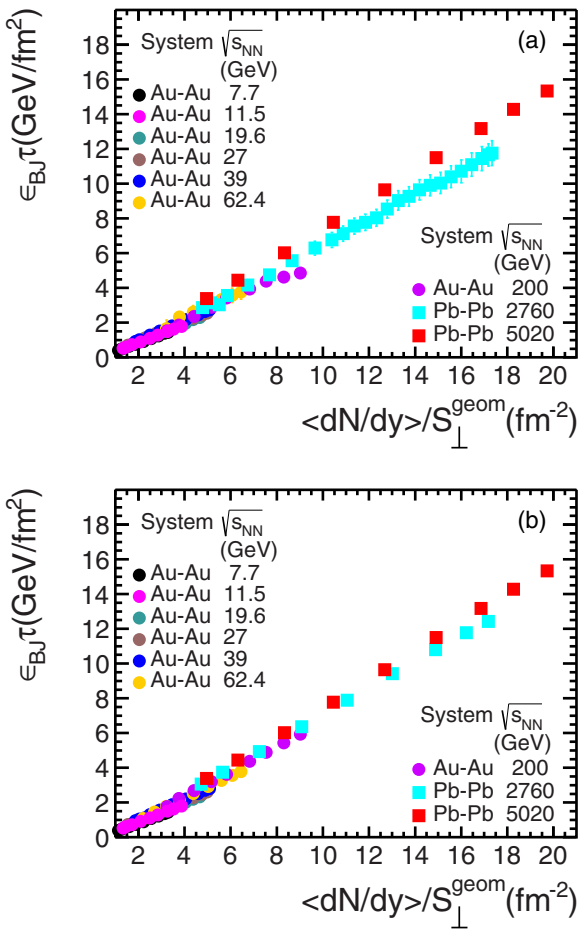

FIG. 12. The Bjorken energy density times the interaction time as a function of $\langle dN/dy\rangle/S_\perp$ for different A-A collision energies and centralities. The difference between panels (a) and (b) is the same as it is explained for Fig. 11.

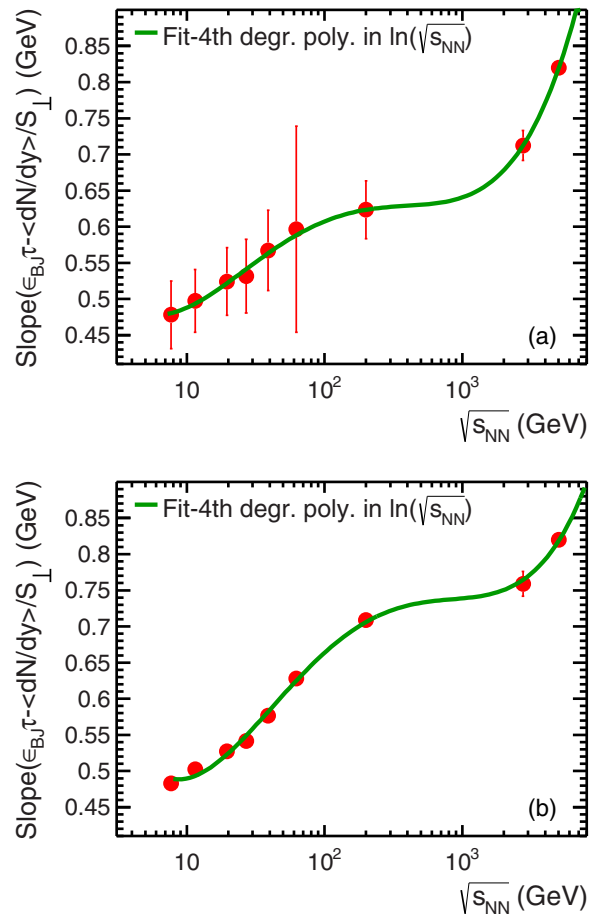

FIG. 13. The slope of the $\epsilon_{Bj}\tau$ linear dependence on $\langle dN/dy\rangle/S_\perp$ as a function of the collision energy. The line is the result of the fit with a fourth-order polynomial in $\ln(\sqrt{s_{NN}})$ and is used to guide the eye. (a) Case I; (b) case II.

VI. SIMILAR STUDIES FOR *pp* MB FOR DIFFERENT COLLISION ENERGIES AND AS A FUNCTION OF $\langle dN/dy\rangle/S_\perp$ AT LHC ENERGIES

The experimental data measured in pp MB collisions [42,54,71–74] at $\sqrt{s} = 62.4$ GeV, 200 GeV, 2.76 TeV, and 5.02 TeV were used for obtaining the $\langle dE_T/dy\rangle/\langle dN/dy\rangle$-$\langle dN/dy\rangle/S_\perp$ correlation considering only $\pi^\pm$, $K^\pm$, p and $\bar{p}$, and the corresponding neutral hadrons in Eqs. (4) and (5). For the BES energies the p_T spectra of the same particles, obtained with an interpolation procedure (INTP) from existing data in this range of energies [75] as explained in Ref. [69], were used. The transverse overlap area was estimated using the Glauber MC approach at subnucleonic level [76]. In Fig. 14 this correlation is presented on top of the results presented in Fig. 4(b). It is seen that the correlation in A-A collisions at different collision energies converges for very peripheral collisions, towards the one corresponding to the pp MB collisions. This is expected so far as towards peripheral A-A collisions the majority of interacting nucleons suffer only single nucleon-nucleon interactions.

At LHC energies, studies of pp collisions up to very high charged-particle multiplicities have shown similarities between pp and Pb-Pb in terms of the behavior of different observables, like near-side long-range pseudorapidity correlations [77], the ($\langle\beta_T\rangle$-$T_{\rm kin}^{\rm fo}$) correlation as a function of charged-particle multiplicity [78], azimuthal angular correlations [79], geometrical scaling [22–24], etc. Experimental data on transverse momentum spectra for light flavors as a function of the average charged-particle multiplicity at LHC energies were published in Refs. [80–82]. The transverse overlap area for pp collisions, $S_\perp^{pp} = \pi r_{\rm max}^2$ as a function of charged-particle multiplicity was estimated using the result of Ref. [83], computed in the IP-Glasma model, $r_{\rm max}$ being the maximal radius for which the energy density of the Yang-Mills fields is above $\varepsilon = \alpha\Lambda_{\rm QCD}^4$ ($\alpha \in [1, 10]$). The model results were fitted with

$$f_{pp} = \begin{cases} 0.387 + 0.0335x + 0.274x^2 - 0.0542x^3 & \text{if } x < 3.4, \\ 1.538 & \text{if } x \geqslant 3.4. \end{cases} \quad (6)$$

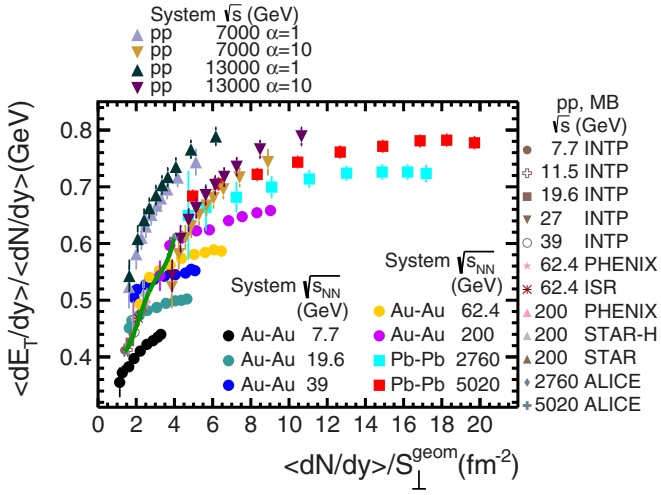

FIG. 14. The $\langle dE_T/dy\rangle/\langle dN/dy\rangle$-$\langle dN/dy\rangle/S_\perp$ correlation for *A*-*A* collisions, case II, *pp* MB at the same energies (the green line, the result of a fourth-order polynomial, guides the eye) and *pp* as a function of charged-particle multiplicity at $\sqrt{s} = 7$ and 13 TeV.

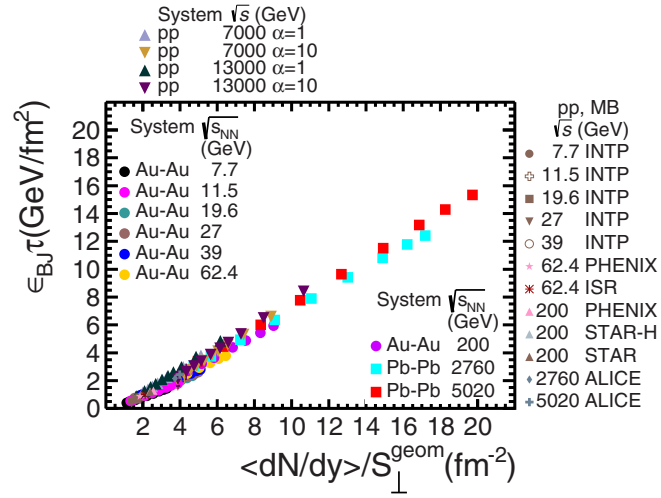

FIG. 15. The same type of figure as Fig. 14, but for the Bjorken energy density times the interaction time as a function of $\langle dN/dy\rangle/S_\perp$.

Using the same recipe we fitted the $r_{\max}$ values from Ref. [83] for $\alpha = 10$ with the following expression:

$$f_{pp} = \begin{cases} -0.18 + 0.3976x + 0.095x^2 - 0.028x^3 & \text{if } x < 3.4, \\ 1.17 & \text{if } x \geqslant 3.4, \end{cases} \tag{7}$$

where $x = (dN/dy)^{1/3}$ and $r_{\max} = 1\,\text{fm} f_{pp}(x)$. The transverse energy per unit rapidity has been estimated using the same procedure as the one used for *A*-*A* collisions at LHC explained in Sec. II. The results in terms of $\langle dE_T/dy\rangle/\langle dN/dy\rangle$-$\langle dN/dy\rangle/S_\perp$ correlations for *pp* collisions at $\sqrt{s} = 7$ and 13 TeV are presented in Fig. 14 for $\alpha = 10$ and $\alpha = 1$. The results corresponding to *pp* collision at $\sqrt{s} = 13$ TeV were obtained within the assumption that the above parametrization of the transverse overlap area does not change significantly. It is seen that the trend of the $\langle dE_T/dy\rangle/\langle dN/dy\rangle$-$\langle dN/dy\rangle/S_\perp$ correlation for *pp* collisions at the LHC energies follows the one of Pb-Pb at $\sqrt{s_{NN}} = 5.02$ TeV, the quantitative agreement being good for $\alpha = 10$ within the same $\langle dN/dy\rangle/S_\perp$ range. For the same values of $\langle dN/dy\rangle/S_\perp$, slightly larger values of $\langle dE_T/dy\rangle/\langle dN/dy\rangle$ in *pp* at $\sqrt{s} = 7$ TeV relative to Pb-Pb at $\sqrt{s_{NN}} = 5.02$ TeV and in *pp* at $\sqrt{s} = 13$ TeV relative to $\sqrt{s} = 7$ TeV are seen. As mentioned in the previous sections, this is in line with the expectations based on the string percolation approach. The Bjorken energy density times the interaction time values for *pp* collisions at the two LHC energies as a function of $\langle dN/dy\rangle/S_\perp$ presented in Fig. 15, using the same symbols as in Fig. 14, are in very good agreement with the ones corresponding to the Pb-Pb collision at $\sqrt{s_{NN}} = 5.02$ TeV.

For *pp* collisions, the slopes of $\epsilon_{Bj}\tau$ as a function of $\langle dN/dy\rangle/S_\perp$ are 0.89 ± 0.09 GeV at $\sqrt{s} = 7$ TeV and 0.92 ± 0.07 GeV at $\sqrt{s} = 13$ TeV, respectively, for $\alpha = 10$, values a bit larger than the value corresponding to the Pb-Pb collision at $\sqrt{s_{NN}} = 5.02$ TeV.

VII. CONCLUSIONS

The behavior of $\langle p_T\rangle/\sqrt{\langle dN/dy\rangle/S_\perp}$ as a function of the collision energy for a given centrality or as a function of centrality for a given collision energy supports the predictions of CGC and percolation based approaches. The dependence of the ratio of the energy density to the entropy density as a function of entropy density at different collision centralities for *A*-*A* collisions from AGS, SPS, RHIC, and LHC energies reveals a tendency towards saturation starting with the largest RHIC energies and a steep rise at the LHC energies. A clear dependence of this behavior on the size of the transverse overlap area is highlighted. The increase in $\langle dE_T/dy\rangle/\langle dN/dy\rangle$ at RHIC energies becomes steeper and the $\langle dN/dy\rangle/S_\perp$ range, which corresponds to a trend close to a plateau, decreases from central to peripheral collisions, converging towards the behavior corresponding to MB *pp* collisions.

In a core-corona scenario, the corona contribution to the observed trends is removed and similar correlations are presented for the core in the case of the identified charged hadrons and their corresponding neutral particles.

The values of the energy density to the entropy density for the same entropy density increase with the collision energy, supporting the expectation based on the string percolation approach.

The Bjorken energy density times the interaction time has a linear dependence on the particle multiplicity per unit rapidity and unit transverse overlap area. The linear dependence also holds for the LHC energies, its slope increasing significantly at these energies, which is an expected trend in the string percolation approach.

The observed trend of the slopes of the $\epsilon_{Bj}\tau$ dependence on the entropy density $\langle dN/dy\rangle/S_\perp$, as a function of the collision energy, is similar to the ones evidenced in the $\langle dE_T/dy\rangle/\langle dN/dy\rangle$-$\langle dN/dy\rangle/S_\perp$ correlations.

The $\langle dE_T/dy\rangle/\langle dN/dy\rangle$-$\langle dN/dy\rangle/S_\perp$ and $\epsilon_{Bj}\tau$-$\langle dN/dy\rangle/S_\perp$ correlations for *pp* collisions at $\sqrt{s} = 7$ and 13 TeV follow qualitatively the ones corresponding to Pb-Pb collisions at $\sqrt{s_{NN}} = 5.02$ TeV. Within the error bars,

there is also a quantitative agreement if for $S_\perp$ for the pp collision as a function of particle density only the region of overlap zone characterized by an energy density larger than $\approx$2 GeV/fm^3 is considered. For pp collisions the slopes corresponding to the $\epsilon_{Bj}\tau$-$\langle dN/dy\rangle/S_\perp$ correlation have values a bit larger than the value corresponding to the Pb-Pb collision at $\sqrt{s_{NN}} = 5.02$ TeV.

ACKNOWLEDGMENTS

This work was carried out under the contracts sponsored by the Ministry of Research, Innovation and Digitization: Contracts No. RONIPALICE-07/03.01.2022 (via Institute of Atomic Physics) and No. PN-19 06 01 03.

[1] G. F. Chapline and A. K. Kerman, On the Possibility of Making Quark Matter in Nuclear Collisions, Preprint CTP-695 MIT-Cambridge - April 1978, available at http://inspirehep.net/record/134446/files/CTP-695.pdf.
[2] J. C. Collins and M. J. Perry, Phys. Rev. Lett. **34**, 1353 (1975).
[3] N. Cabibbo and G. Parisi, Phys. Lett. B **59**, 67 (1975).
[4] E. V. Shuryak, Phys. Lett. B **78**, 150 (1978).
[5] G. Baym, Phys. A (Amsterdam, Neth.) **96**, 131 (1979).
[6] T. Celik *et al.*, Phys. Lett. B **97**, 128 (1980).
[7] L. McLerran and R. Venugopalan, Phys. Rev. D **49**, 2233 (1994).
[8] L. McLerran and R. Venugopalan, Phys. Rev. D **49**, 3352 (1994).
[9] L. McLerran and R. Venugopalan, Phys. Rev. D **50**, 2225 (1994).
[10] E. Iancu, A. Leonidov, and L. McLerran, Nucl. Phys. A **692**, 583 (2001).
[11] A. Mazeliauskas, Nucl. Phys. A **982**, 134 (2019), and references therein.
[12] L. Van Hove, Phys. Lett. B **118**, 138 (1982).
[13] B. Mohanty, Jan-e Alam, S. Sarkar, T. K. Nayak, and B. K. Nandi, Phys. Rev. C **68**, 021901(R) (2003).
[14] L. Adamczyk *et al.* (STAR Collaboration), Phys. Rev. C **96**, 044904 (2017).
[15] J. P. Blaizot and J. Y. Ollitrault, Nucl. Phys. A **458**, 745 (1986).
[16] J. P. Blaizot and J. Y. Ollitrault, Phys. Lett. B **191**, 21 (1987).
[17] S. S. Adler *et al.* (PHENIX Collaboration), Phys. Rev. C **71**, 034908 (2005).
[18] J. Adam *et al.* (ALICE Collaboration), Phys. Rev. C **94**, 034903 (2016).
[19] A. Adare *et al.* (PHENIX Collaboration), Phys. Rev. C **93**, 024901 (2016).
[20] B. Sharma, Transverse energy analysis of Au+Au collisions at 7.7, 11.5, 19.6, 27, and 39 GeV through the use of identified particles spectra, Master's thesis, University of Tennessee, 2018, https://trace.tennessee.edu/utk_gradthes/5118.
[21] A. Monnai and J. Y. Ollitrault, Phys. Rev. C **96**, 044902 (2017).
[22] M. Petrovici, A. Lindner, A. Pop, M. Tarzila, and I. Berceanu, Phys. Rev. C **98**, 024904 (2018), and references therein.
[23] M. Petrovici, A. Lindner, and A. Pop, in *Exotic Nuclei and Nuclear/Particle Astrophysics (VII): Physics with Small Accelerators: Proceedings of the Carpathian Summer School of Physics 2018 (CSSP18)*, AIP Conf. Proc. Vol. 2076 (AIP, New York, 2019), p. 040001.
[24] A. Lindner, M. Petrovici, and A. Pop, Proc. Sci. (PoS) **380**, 197 (2021), Particles and Nuclei International Conference (PANIC2021), https://pos.sissa.it/380/197/.
[25] R. J. Glauber, Phys. Rev. **100**, 242 (1955).
[26] V. Franco and R. J. Glauber, Phys. Rev. **142**, 1195 (1966).
[27] M. L. Miller *et al.*, Annu. Rev. Nucl. Part. Sci. **57**, 205 (2007).
[28] M. Rybczynski, G. Stefanek, W. Broniowski, and P. Bozek, Comput. Phys. Commun. **185**, 1759 (2014).
[29] E. Iancu, A. Leonidov, and L. McLarren, *The Colour Glass Condensate: An Introduction*, edited by J. P. Blaizot and E. Iancu, QCD Perspectives on Hot and Dense Matter, NATO Science Series, Vol. 87 (Springer, Dordrecht, 2002); E. Ferreiro, E. Iancu, A. Leonidov, and L. McLarren, Nucl. Phys. A **703**, 489 (2002).
[30] D. Kharzeev, E. Levin, and M. Nardi, Nucl. Phys. A **730**, 448 (2004); **743**, 329 (2004); Phys. Rev. C **71**, 054903 (2005); D. Kharzeev and M. Nardi, Phys. Lett. B **507**, 121 (2001); D. Kharzeev, E. Levin, and L. McLarren, Nucl. Phys. A **748**, 627 (2005); Phys. Lett. B **561**, 93 (2003).
[31] Y. L. Dokshitzer, V. A. Khoze, and S. Troian, J. Phys. G: Nucl. Part. Phys. **17**, 1585 (1991).
[32] E. Levin and A. H. Rezaeian, Phys. Rev. D **83**, 114001 (2011).
[33] T. Lappi, Eur. Phys. J. C **71**, 1699 (2011).
[34] T. S. Biro, H. B. Nielsen, and J. Knoll, Nucl. Phys. B **245**, 449 (1984).
[35] J. Dias de Deus and C. Pajares, Phys. Lett. B **695**, 211 (2011).
[36] V. Topor Pop and M. Petrovici, Phys. Rev. C **98**, 064903 (2018).
[37] A. H. Mueller, Nucl. Phys. A **715**, 20c (2003).
[38] L. V. Gribov, E. M. Levin, and M. G. Ruskin, Phys. Rep. **100**, 1 (1983), and references therein.
[39] H1 Collaboration, Nucl. Phys. B **470**, 3 (1996).
[40] ZEUS Collaboration, Eur. Phys. J. C **7**, 609 (1999), and references therein.
[41] H1 Collaboration, Eur. Phys. J. C **64**, 561 (2009).
[42] B. I. Abelev *et al.* (STAR Collaboration), Phys. Rev. C **79**, 034909 (2009).
[43] R. Sahoo (STAR Collaboration), Indian J. Phys. **85**, 897 (2011).
[44] R. Sahoo *et al.*, Rom. Rep. Phys. **58**, 055 (2006).
[45] J. Adams *et al.* (STAR Collaboration), Phys. Rev. C **70**, 054907 (2004).
[46] S. Chatterjee *et al.*, Adv. High Energy Phys. **2015**, 349013 (2015).
[47] J. Adam *et al.* (STAR Collaboration), Phys. Rev. C **102**, 034909 (2020).
[48] M. M. Aggarwal *et al.* (STAR Collaboration), Phys. Rev. C **83**, 024901 (2011).
[49] J. Adams *et al.* (STAR Collaboration), Phys. Rev. Lett. **98**, 062301 (2007).
[50] G. Agakishiev *et al.* (STAR Collaboration), Phys. Rev. Lett. **108**, 072301 (2012).
[51] B. Abelev *et al.* (ALICE Collaboration), Phys. Rev. C **88**, 044910 (2013).
[52] B. Abelev *et al.* (ALICE Collaboration), Phys. Rev. Lett. **111**, 222301 (2013).
[53] B. Abelev *et al.* (ALICE Collaboration), Phys. Lett. B **728**, 216 (2014); **734**, 314 (2014).

[54] S. Acharya *et al.* (ALICE Collaboration), Phys. Rev. C **101**, 044907 (2020).
[55] D. S. de Albuquerque, Multi-strange hadrons in Pb–Pb collisions at the LHC with ALICE, Ph.D. thesis, 2019, CERN-THESIS-2019-135.
[56] P. Kalinak (ALICE Collaboration), European Physical Society Conference on High Energy Physics, 5–12 July 2017, Venice, Italy, PoS(EPS-HEP2017)168 (2017), https://pos.sissa.it/314/168/pdf.
[57] D. S. de Albuquerque (ALICE Collaboration), Nucl. Phys. A **982**, 823 (2019), XXVIIth International Conference on Ultra-relativistic Nucleus-Nucleus Collisions (Quark Matter 2018).
[58] S. Pal and S. Pratt, Phys. Lett. B **578**, 310 (2004).
[59] J. Braun, B. Klein, H. J. Pirner, and A. H. Rezaeian, Phys. Rev. D **73**, 074010 (2006).
[60] Bo-Liu Li *et al.*, Nucl. Phys. B **938**, 298 (2019).
[61] Z. Arnold *et al.*, Solid State Commun. **92**, 807 (1994).
[62] P. Bożek, Acta Phys. Pol. B **36**, 3071 (2005).
[63] K. Werner, Phys. Rev. Lett. **98**, 152301 (2007).
[64] F. Becattini and J. Manninen, J. Phys. G: Nucl. Part. Phys. **35**, 104013 (2008).
[65] J. Aichelin and K. Werner, Phys. Rev. C **79**, 064907 (2009); **81**, 029902(E) (2010); J. Phys. G: Nucl. Part. Phys. **37**, 094006 (2010).
[66] P. Bozek, Phys. Rev. C **79**, 054901 (2009).
[67] M. Gemard and J. Aichelin, Astron. Nachr. **335**, 660 (2014).
[68] M. Petrovici, I. Berceanu, A. Pop, M. Tarzila, and C. Andrei, Phys. Rev. C **96**, 014908 (2017).
[69] A. Pop and M. Petrovici (unpublished).
[70] J. D. Bjorken, Phys. Rev. D **27**, 140 (1983).
[71] A. Adare *et al.* (PHENIX Collaboration), Phys. Rev. C **83**, 064903 (2011).
[72] J. Adams *et al.* (STAR Collaboration), Phys. Lett. B **616**, 8 (2005).
[73] J. Adams *et al.* (STAR Collaboration), Phys. Lett. B **637**, 161 (2006).
[74] B. Abelev *et al.* (ALICE Collaboration), Phys. Lett. B **736**, 196 (2014).
[75] B. Alper *et al.* (British-Scandinavian Collaboration), Nucl. Phys. B **100**, 237 (1975).
[76] P. Bozek, W. Broniowski, M. Rybczynski, and G. Stefanek, Comput. Phys. Commun. **245**, 106850 (2019).
[77] V. Khachatryan *et al.* (CMS Collaboration), J. High Energy Phys. 09 (2010) 091.
[78] C. Andrei, ALICE Collaboration, Nucl. Phys. A **931**, 888 (2014).
[79] V. Khachatryan *et al.* (CMS Collaboration), Phys. Lett. B **765**, 193 (2017).
[80] S. Acharya *et al.* (ALICE Collaboration), Phys. Rev. C **99**, 024906 (2019).
[81] S. Acharya *et al.* (ALICE Collaboration), Eur. Phys. J. C **80**, 693 (2020).
[82] S. Acharya *et al.* (ALICE Collaboration), Eur. Phys. J. C **80**, 167 (2020).
[83] A. Bzdak, B. Schenke, P. Tribedy, and R. Venugopalan, Phys. Rev. C **87**, 064906 (2013).